

R1 ANL/CP--76545
DE92 017067 T1

FROM SUPERDEFORMATION TO CLUSTERS*

R. R. Betts

Physics Division

Argonne National Laboratory

Argonne, IL 60439

DISCLAIMER

This report was prepared as an account of work sponsored by an agency of the United States Government. Neither the United States Government nor any agency thereof, nor any of their employees, makes any warranty, express or implied, or assumes any legal liability or responsibility for the accuracy, completeness, or usefulness of any information, apparatus, product, or process disclosed, or represents that its use would not infringe privately owned rights. Reference herein to any specific commercial product, process, or service by trade name, trademark, manufacturer, or otherwise does not necessarily constitute or imply its endorsement, recommendation, or favoring by the United States Government or any agency thereof. The views and opinions of authors expressed herein do not necessarily state or reflect those of the United States Government or any agency thereof.

***Invited Paper Presented at International Conference on Nuclear
Structure at High Angular Momentum, Ottawa, Canada, May 18-21, 1992**

JMB
DISTRIBUTION OF THIS DOCUMENT IS UNLIMITED

MASTER

The submitted manuscript has been authored by a contractor of the U. S. Government under contract No. W-31-109-ENG-38. Accordingly, the U. S. Government retains a nonexclusive, royalty-free license to publish or reproduce the published form of this contribution, or allow others to do so, for U. S. Government purposes.

FROM SUPERDEFORMATION TO CLUSTERS

R. R. Betts

Physics Division, Argonne National Lab., Argonne, IL 60439

Much of the discussion at this conference has centered on the topic of superdeformed states in nuclei, and their study with the exquisitely precise tool of gamma ray spectroscopy, carried out with state-of-the-art detector arrays. In the usual way in which superdeformed states are populated, via compound nucleus formation and evaporation, gamma decay is the last process to occur in the decay chain. In some other sense, it is also the last to occur in the meaning of least likely. Figure 1 illustrates schematically the

ANL-P-20710

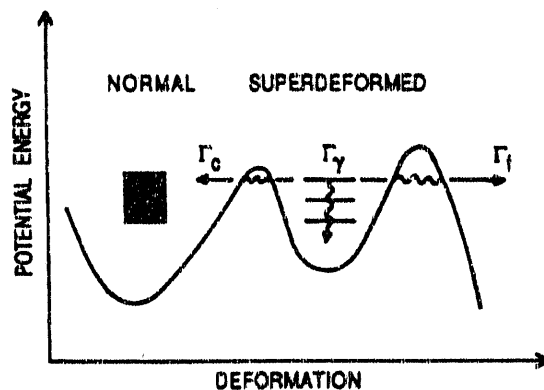


Fig. 1. Schematic representation of the potential energy of a nucleus as a function of deformation. The different contributions to the decay widths of quasi-stable states in the superdeformed minimum are indicated.

potential energy surface of a nucleus as a function of deformation showing the quasi-stable states which exist in the secondary superdeformed minimum at large deformations. Several components contribute to the total decay width of states in this secondary minimum. They are, respectively; Γ_γ , the gamma decay width; Γ_f , the fission or particle decay width and Γ_c , the width for decay into states of normal structure. The natural units which set the scale for each of these components are: for Γ_γ , the Weisskopf unit which, for a 1 MeV E2 transition in a mass 150 nuclei gives $\Gamma_\gamma \approx 4 \times 10^{-5}$ eV and for Γ_f , the Wigner limit which, roughly, for symmetric breakup gives values of several keV. Thus, we see that, in order for gamma decay of superdeformed states to occur, not only must the gamma decay width be tremendously enhanced by the collective rotation of the system, but the fission decay width must be enormously suppressed by penetration through the outer part of the two-humped fission barrier. This, of course, is obviously the case in those nuclei in which we have been able to observe gamma-decaying states, but there is an implication that a much wider area of study for superdeformation may be available with modes other than gamma decay.

The first evidence for superdeformation came from the observation of isomeric fissioning states in very heavy nuclei. These superdeformed states were populated via the compound nucleus formed in neutron capture, which then couples to the superdeformed minimum through Γ_C , and fissions through Γ_f . The exact details of this process depend on the relative values of Γ_C and Γ_f and on the level densities of normal and superdeformed states. One case which is of interest in the context of the present discussion is, perhaps prophetically, mentioned in Bohr and Mottelson Vol. II¹⁾ corresponding to the situation where $\Gamma_f \gg \Gamma_C$ when the total width of the superdeformed states is much larger than the average width of normal states. In this situation; *"The broad type II (superdeformed) state would strongly manifest itself in the hypothetical fission fragment scattering process."* This is the subject of this talk.

Fission fragment scattering may be thought of as the ultimate radioactive beam experiment. The fission fragments from heavy nuclei are produced in highly excited states and therefore any attempt to observe superdeformed states via the inverse of their fission decay might seem fruitless. This is emphasized in Fig. 2,

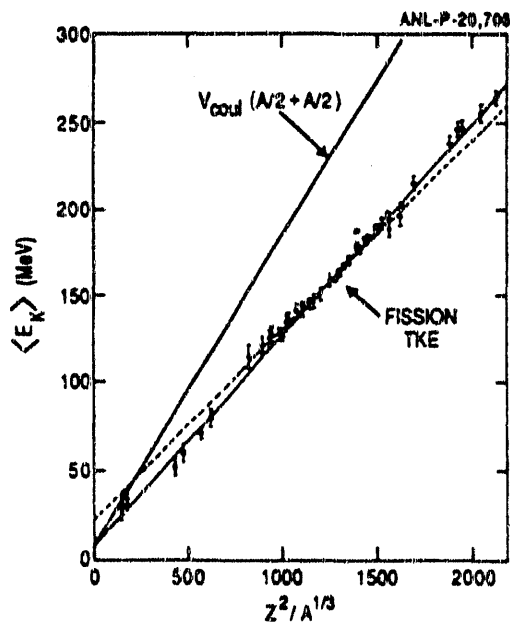


Fig. 2. Systematics of fission fragment kinetic energies compared with the Coulomb barrier for spherical fragments.

which shows the systematics of fission fragment kinetic energies plotted as a function of $Z^2/A^{1/3}$ due to Viola²⁾, compared with the Coulomb energy for touching spheres of mass $A/2$. For heavier systems, the difference between the fragment kinetic energies and the spherical Coulomb barrier reflects the large deformations of the fission fragments at scission and underlines the essential impossibility of mimicking the time-reversal fission process through collision processes. For much lighter systems, however, the fragment kinetic energies lie much closer to the spherical Coulomb barrier, reflecting the shape transition predicted by the liquid drop model³⁾ to a scission point configuration close to two touching

spheres. In these cases, therefore, we expect that scattering processes may indeed be similar to inverse fission of the compound nucleus. This observation opens up the possibility of studying regions of superdeformation predicted to occur for $Z < 40$, $A < 80$ which can be accessed via a variety of scattering channels.

The above ideas provide a useful vehicle for discussion of some features of a wide variety of data on scattering and reactions of light nuclei. One striking example⁴⁾ of this is shown in Figs. 3-5. In Fig. 3, the angular distribution of elastic scattering of $^{28}\text{Si} + ^{28}\text{Si}$

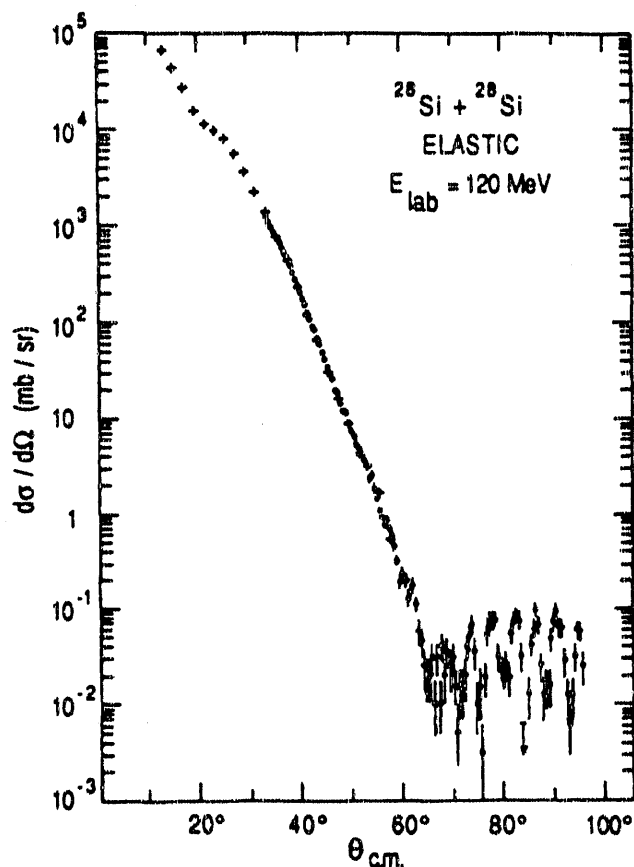


Fig. 3. Angular distribution of elastic scattering of $^{28}\text{Si} + ^{28}\text{Si}$ at a bombarding energy of 120 MeV.

^{28}Si at a bombarding energy of roughly twice the Coulomb barrier is shown. At forward angles, the data show a typical transition from Coulomb scattering through nuclear-Coulomb interference to a steep fall-off characteristic of the scattering of strongly absorbing particles. These features are readily described with a variety of optical model calculations. At the largest angles, however, the data show an abrupt transition to a highly oscillatory behavior similar to that of a pure Legendre polynomial squared of order $L = 40$ which, in this case, is the grazing angular momentum. In the large-angle region, the elastic scattering channel is relatively weak as demonstrated by the spectrum shown in Fig. 4 which shows

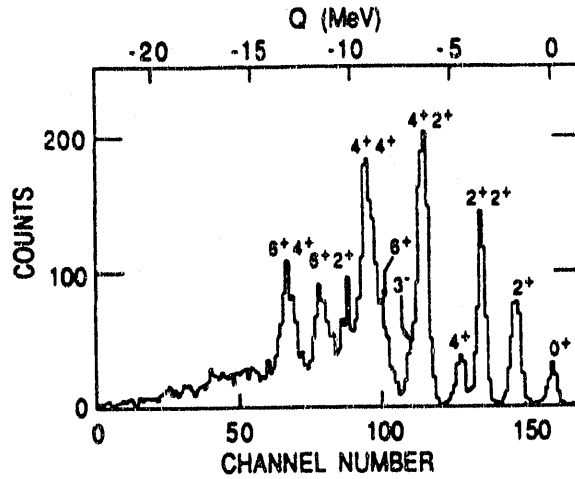


Fig. 4. Spectrum of $^{28}\text{Si} + ^{28}\text{Si}$ at large angles measured at a bombarding energy of 120 MeV.

strong excitation of inelastic and mutual inelastic channels. These channels show the same general angular behavior as do the elastics as displayed in Fig. 5. Namely, a forward angle dependence of the

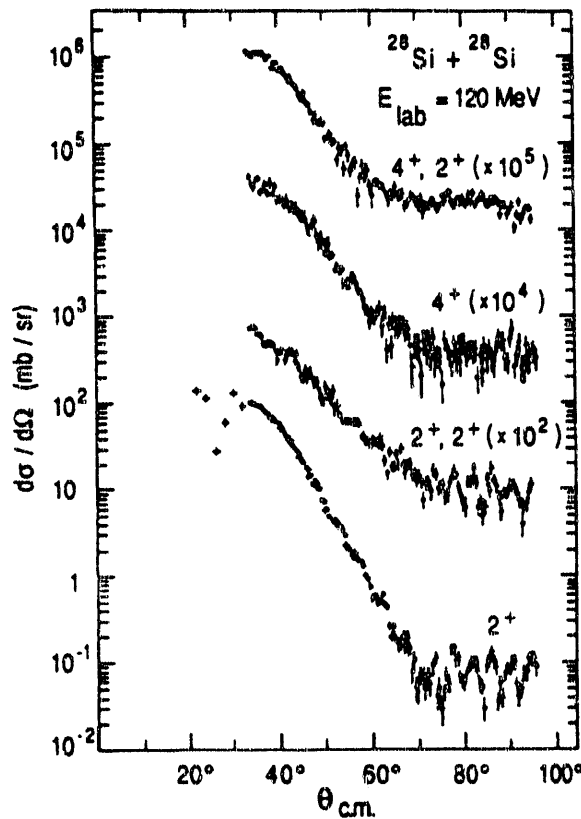


Fig. 5. Angular distributions of inelastic and mutual inelastic scattering of $^{28}\text{Si} + ^{28}\text{Si}$ at a bombarding energy of 120 MeV.

cross-section characteristic of Coulomb and nuclear scattering with strong absorption, and a large-angle behavior suggesting the presence of a much longer time-scale process.

The demonstration of the long time-scale involved in the large angle cross-sections comes from the data⁵⁾ shown in Fig. 6 which

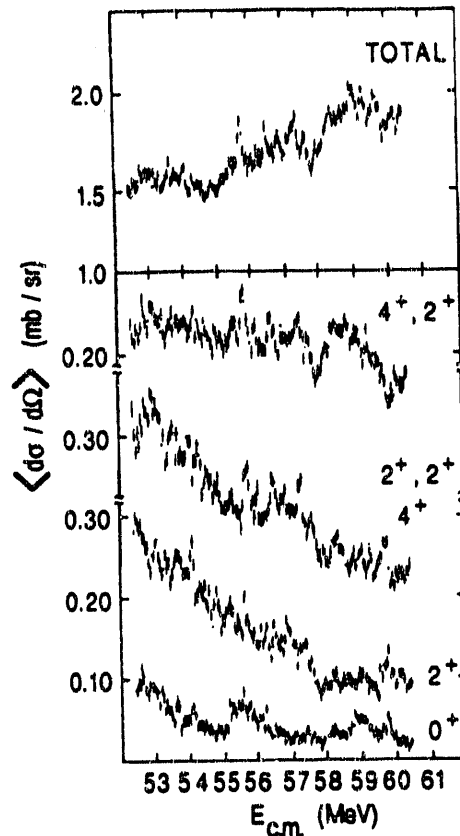


Fig. 6. Excitation functions for elastic and inelastic scattering of $^{28}\text{Si} + ^{28}\text{Si}$ showing many correlated structures of width 100-200 keV.

displays the energy dependence of the large angle cross-sections measured in center-of-mass energy steps of 50 keV. The narrow structures observed in this cross-section have been demonstrated⁶⁾ to correspond to a complex pattern of isolated resonances in the composite system with angular momenta, obtained from elastic scattering angular distributions⁷⁾, ranging from 36-40 \hbar . These resonances, which appear with an average spacing of 300 keV lie in a region of excitation energy and angular momentum from which the level density of the compound nucleus, ^{56}Ni , is calculated to be several thousand per MeV. Conversely, their decay widths into the symmetric channel ($^{28}\text{Si} + ^{28}\text{Si}$) are on the order of keV whereas the average compound nuclear state has a statistical decay width into these channels of only eV. It is clear therefore, that these resonances correspond to a rather special subset of states stabilized against mixing into the more numerous compound nucleus states by some special symmetry.

Information on the origin of this special stability comes from data⁴⁾ for $^{28}\text{Si} + ^{30}\text{Si}$ and $^{30}\text{Si} + ^{30}\text{Si}$ shown in comparison with $^{28}\text{Si} + ^{28}\text{Si}$ in Fig. 7. The addition of neutrons not only results in a

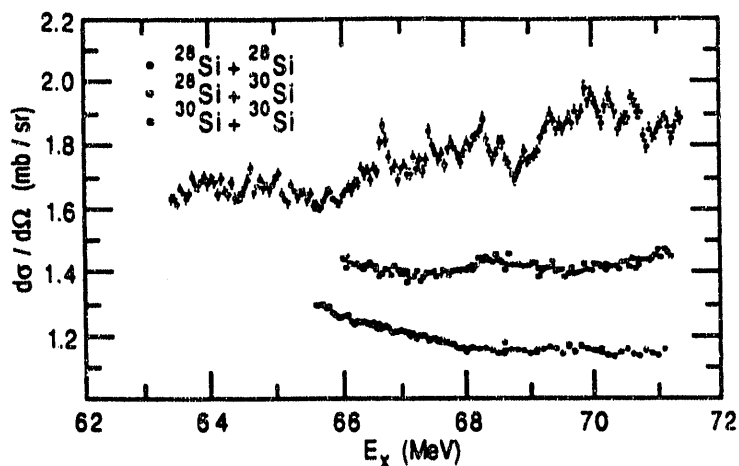


Fig. 7. Total large-angle cross sections for scattering and reactions of $^{28}\text{Si} + ^{28}\text{Si}$, $^{28}\text{Si} + ^{30}\text{Si}$ and $^{30}\text{Si} + ^{30}\text{Si}$ as a function of compound nucleus excitation energy.

disappearance of the prominent narrow structures, but also in a suppression of the total cross-sections by factors of two and four respectively. The general behavior of these cross-sections, as well as the mass distributions are quite consistent with the origin of these processes being fission of the compound nucleus. In which case, the disappearance of the narrow structures may be associated with the disappearance of a shell-stabilized secondary minimum which occurs with the addition of neutrons. These data, therefore, provide evidence for superdeformation in the mass 56 region.

It should be hoped that one could proceed from these observations to a spectroscopy which would then further test the hypothesis. The pattern of resonances is, however, extremely complex and we lack evidence for unifying features of the data such as rotational bands which appear in such a direct way in the gamma-ray studies. For other systems, such as $^{24}\text{Mg} + ^{24}\text{Mg}$ ⁸⁾ shown in Fig. 8 there is an apparently simpler behavior, with similar groups of

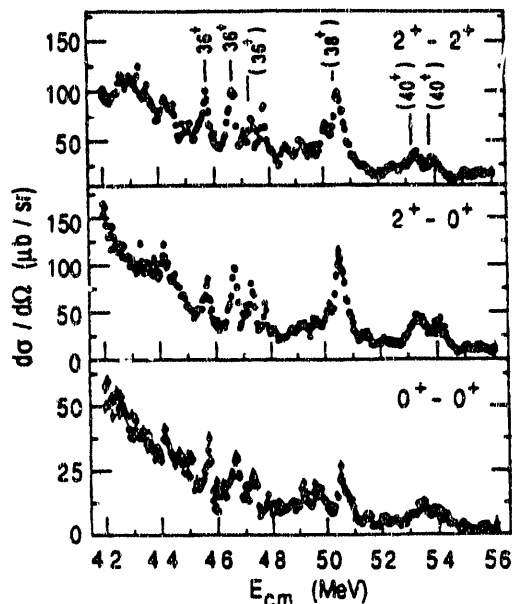


Fig. 8. Excitation functions for elastic and inelastic scattering of $^{24}\text{Mg} + ^{24}\text{Mg}$.

resonances appearing for each spin^{8,9}). It is therefore of interest to look at some models to see if any such features appear in a simple way. In this case, the deformed harmonic oscillator provides a useful starting point which may have some validity in these light nuclei. Note here, that Nilsson-Strutinsky calculations¹⁰) using deformed oscillator shell corrections predict a 3:1 hyperdeformed minimum for ⁴⁸Cr at angular momenta appropriate to the ²⁴Mg + ²⁴Mg scattering data.

The energy levels of an axially deformed harmonic oscillator are shown in Fig. 9 plotted versus deformation. Shell gaps appear

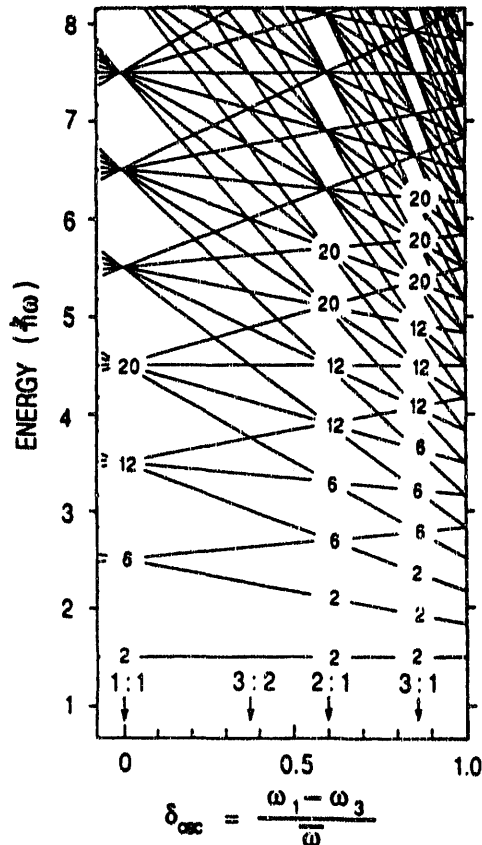


Fig. 9. Energy levels of an axially deformed harmonic oscillator with the degeneracies of the shells which occur at integer ratios of the frequencies.

at deformations corresponding to integer ratios of the frequencies along and perpendicular to the deformation axis. Also shown are the degeneracies of the orbits at these values of the deformation. For 2:1 deformation we see a doubling of the spherical degeneracies, for 3:1 a tripling and so on. It has been shown¹¹) that these sets of degenerate orbits have the same SU(3) symmetry as do the spherical shells and a decomposition of the deformed oscillator wavefunctions at these deformations into "multi-clusters" has been proposed. These authors were careful to point out that the use of the word "cluster" was not to be taken in the usual sense, as such true clustering would be strongly inhibited by the Pauli principle. A closer look at the details of the wavefunctions, however, reveals a

possible connection between the deformed oscillator and clustering. For example, for the 2:1 shape, the quantum numbers of the degenerate orbits fall into two groups:

<u>Degeneracy</u>	<u>Sphere</u>	<u>[N N₃]</u>	<u>2:1</u>
2	[0,0]	[0,0]	[0,1]
6	[1,0]	[1,0]	[1,1]
	[0,1]	[0,2]	[0,3]
12	[2,0]	[2,0]	[2,1]
	[1,1]	[1,2]	[1,3]
	[0,2]	[0,4]	[0,5]
	[N N ₃]	[N 2N ₃]	[N 2N ₃ +1]

This connection between the spherical quantum numbers and those at the 2:1 shape is precisely that which comes from the evolution of a two-center shell model into a single center potential, provided that this evolution takes place adiabatically. The origin of this is illustrated schematically in Fig. 10 where the evolution of the

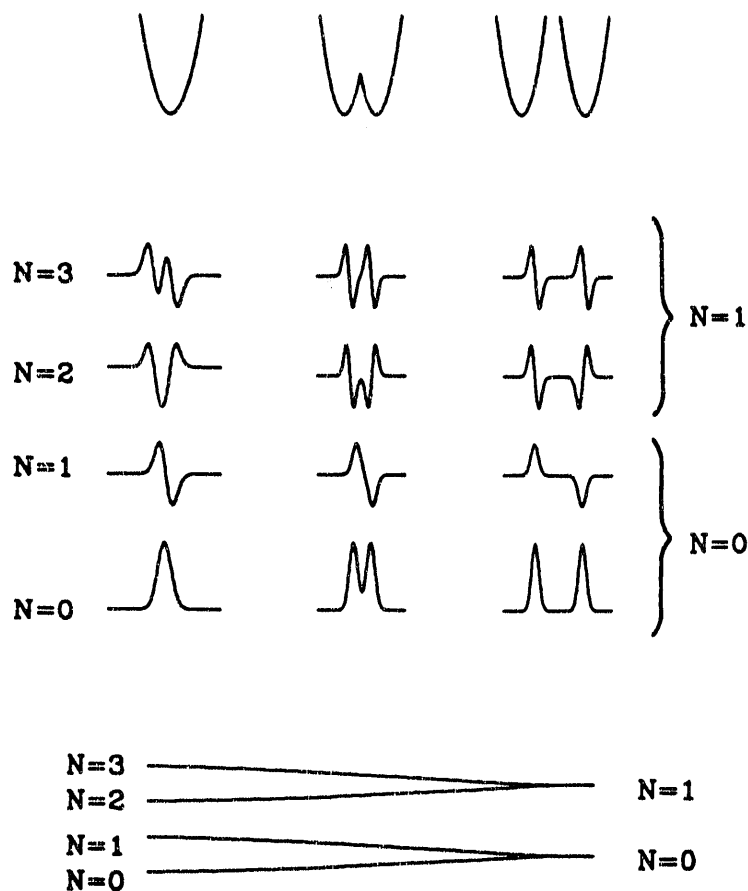


Fig. 10. Evolution of the potential, wavefunctions and energies of a symmetric two center harmonic oscillator.

wavefunctions and energy levels in a two-center model are shown as a function of separation of the two centers. In the symmetric two-center case, the requirement that the wavefunction have good parity results in an initially degenerate pair of states with positive and negative parity which split as the two centers merge. In this way the quantum number N of the single center potential wavefunctions evolves to either $2N$ or $2N+1$, exactly as is the case for the 2:1 oscillator. These ideas may be generalized to the $N:1$ oscillator and the N -center shell model and also to cases of non-axial symmetry. The general conclusion is that states in the secondary minima created by the degeneracies which occur in the deformed shell model with rational ratios of axes will, if allowed to do so adiabatically, naturally evolve into clusters suggested by the $SU(3)$ symmetries of the deformed shells. Thus, although the overlaps of the deformed wavefunctions with the clusters may not be large, they contain the correct symmetries for the dynamical evolution of the system into many-center states which have complete overlap with the clusters. In this way, the parentage of highly deformed states can be identified and selection rules for their decay determined.

The above discussion provides some new insight into the comparison of the results of a multi-center shell model calculation¹²⁾ of six alpha-particles with a Nilsson-Strutinsky calculation¹³⁾ of ^{24}Mg . The results of these two calculations are shown in Fig. 11 where the deformed shell model potential energy

ANL-P-18,417

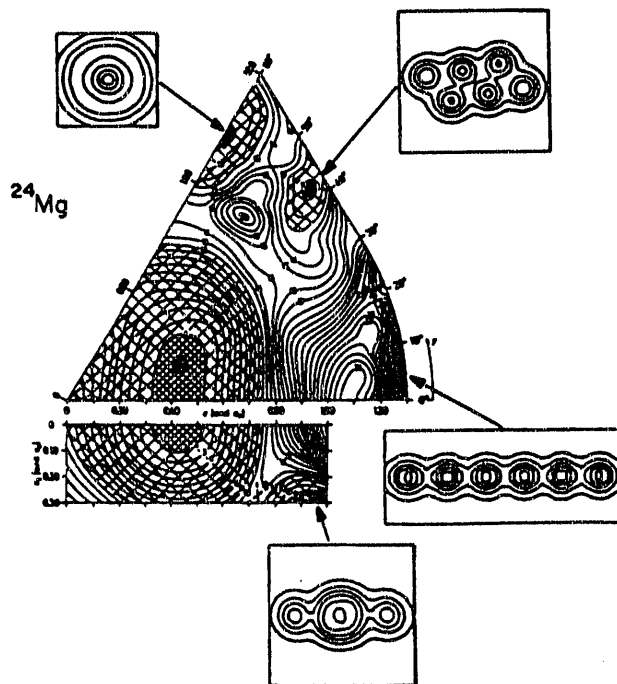


Fig. 11. Comparison between the potential energy surface of ^{24}Mg from a deformed shell model calculation and density contours of cluster states from a multi-center cluster model calculation.

surface is compared with the density contours of quasi-stable configurations of six alpha-particles from the many center shell model calculations. It is possible to make a one-to-one correspondence between the two calculations in a way which gives new order to the variety of resonance phenomena seen in reactions leading to ^{24}Mg . The triaxial minimum ($\epsilon = 1.1$, $\gamma = 40^\circ$) is seen to correspond to a cluster configuration which has the symmetry of two ^{12}C (ground-state) triangles and should therefore be identified with the family of broad resonances seen in $^{12}\text{C} + ^{12}\text{C}$ elastic and inelastic scattering¹⁴). The reflection asymmetric minimum ($\epsilon = 1.0$, $\gamma = 0^\circ$, $\epsilon_3 = 0.30$) has a rather complex structure, with overlap with $^{20}\text{Ne} + \alpha$, $^{16}\text{O} + ^8\text{Be}$ as well as $^{12}\text{C} + ^{12}\text{C}$ channel. This configuration is the basis of the original¹⁵) $^{12}\text{C} + ^{12}\text{C}$ barrier resonances and has also been recently, and elegantly, studied¹⁶) via ^{24}Mg breakup reactions.

In these recent experiments, a beam of ^{24}Mg bombarded a ^{12}C target and ^{12}C fragments were detected and identified at forward angles. From their energies and angles, events corresponding to breakup in which all three participating ^{12}C nuclei are in their ground states were selected and the excitation energy of the ^{24}Mg decaying to two ^{12}C determined. Thus resulting spectrum is shown in Fig. 12. This spectrum is quite similar to the spectrum of

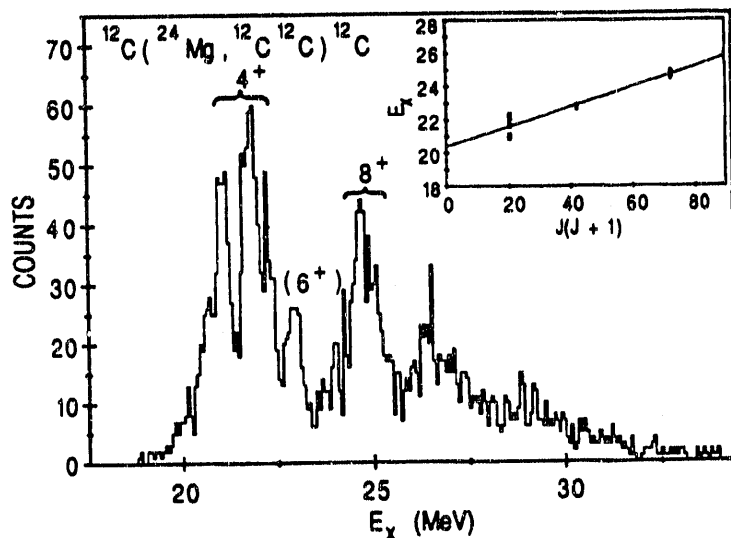


Fig. 12. Excitation energy spectrum of ^{24}Mg states which break up into two ^{12}C (g.s.). The inset shows the rotational band formed by these states.

resonances observed in $^{12}\text{C} + ^{12}\text{C}$ reactions¹⁷) in the same excitation energy region. From the angular correlations of the two breakup ^{12}C it is possible to deduce the resonance spins¹⁸) which, as shown in the inset, lie quite nicely on a rotational band with a moment of inertia of 60 keV, compared to 94 keV predicted from the multi-center shell model, and 74 keV from the deformed shell model.

Finally, both the deformed shell model and multi-center shell model predict the rather exotic configuration with a 6:1 axis ratio corresponding to a linear chain of alpha-particles to be stable.

Phase space and structural considerations lead us to expect that states of this configuration will split into two three alpha-particle chains which, in the cluster model, correspond to the 7.65 MeV O_2^+ state in ^{12}C . The O_2^+ state in ^{12}C is itself unstable to decay into alpha + 8Be and we therefore expect the ^{24}Mg chain configuration to result in six alpha particles produced in a kinematically correlated fashion via the above sequential route. The detection and characterization of a six particle final state is in itself a formidable challenge. A search for this signature of the chain configuration has been carried out¹⁹⁾, using an array of double-sided silicon strip detectors which allow the simultaneous detection of several particles with good energy and spatial resolution²⁰⁾. A beam of ^{12}C was used to bombard a ^{12}C target - the resulting particles were detected on either side of the beam axis with two 5 x 5 cm, 256 quasi-pixel, strip detectors. The resulting excitation spectrum calculated from events in which three alpha-particles hit a single detector is shown in Fig. 13, showing the

ANL-P-20,709

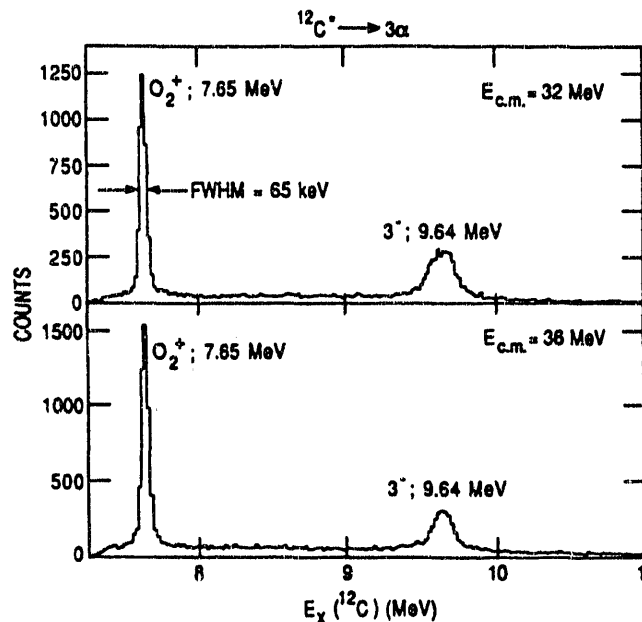


Fig. 13. Excitation spectrum of ^{12}C for events in which three alpha particles are detected in one strip detector.

7.65 MeV O_2^+ in ^{12}C . For events in which three alpha-particles were detected in each of the strip detectors, the total excitation energy spectrum shown in Fig. 14 clearly shows the double excitation of the O_2^+ channel, the sought after decay mode of the ^{24}Mg chain. The cross-section for this channel is shown as a function of energy in Fig. 15 and exhibits a pronounced broad structure centered at $E_{c.m.} = 32.5$ MeV corresponding to an excitation energy of 46.4 MeV in ^{24}Mg with a width of approximately 5 MeV. Subsequent detailed measurements of the angular distributions over the resonance show that, whereas the structure is not characterized by a single angular momentum and therefore corresponds to a number of overlapping resonances, it does appear to be dominated by angular momenta in the vicinity of 14-16 \hbar . Thus, the observed structure lies very close to the predicted crossing of the rotational band based on the chain

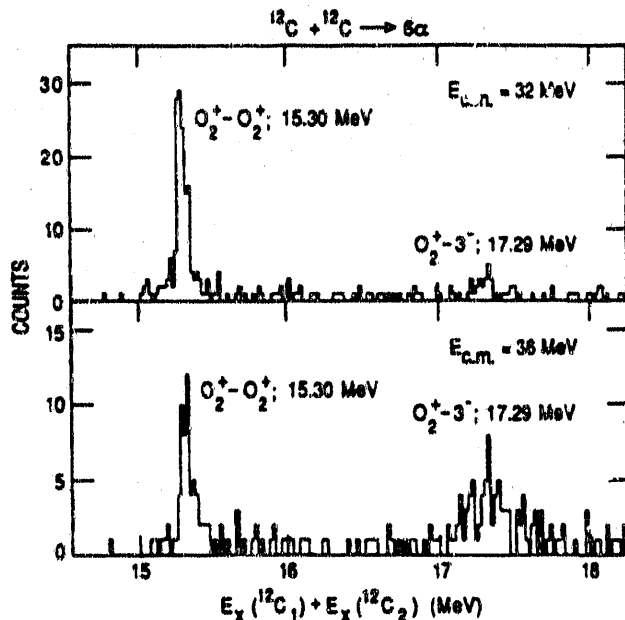


Fig. 14. Total excitation spectrum for events in which six alpha particles are detected, clearly showing the double O_2^+ excitation.

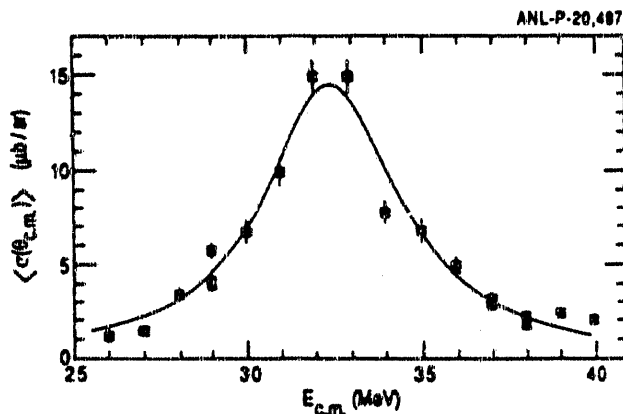


Fig. 15. Cross-section for the double O_2^+ excitation shown as a function of bombarding energy.

configuration with the $^{12}\text{C} + ^{12}\text{C}$ grazing trajectory, as illustrated in Fig. 16. Further experiments and analysis are clearly necessary to substantiate these suggestions but the data are quite consistent with the observation of these extremely unusual configurations of alpha-particle chains.

In summary, there exists clear evidence for the existence of shell effects at extreme deformations in light nuclei studied via fission and cluster decay. The connection between the deformed shell model and the multi-center shell model can be exploited to give insight into the cluster structure of these extremely deformed states and also give hope for a spectroscopy based on selection rules for cluster decays which come from this connection. A clear handicap is, however, at this stage, our inability to make this spectroscopy more quantitative through calculation of the cluster decay widths. Finally, it is also apparent that the introduction of

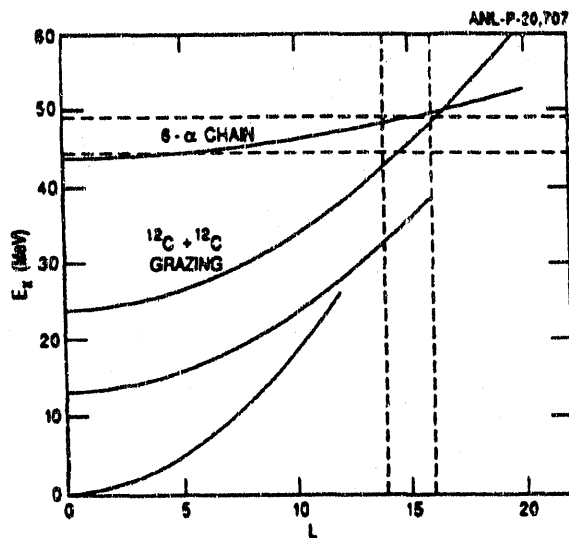


Fig. 16. Plot of excitation energy versus spin for ^{24}Mg showing the predicted location of the six-alpha chain band and its crossing with the $^{12}\text{C} + ^{12}\text{C}$ grazing trajectory. The location of the broad structure observed in the double 0_2^+ channel is indicated by the dashed lines.

a new generation of high segmentation, high resolution particle arrays has and will have a major impact on this aspect of the study of nuclear structure at extreme deformations.

Collaboration and discussions with Martin Freer and Alan Wuosmaa during the preparation of this talk are gratefully acknowledged. This work is supported by the U.S. Department of Energy, Nuclear Physics Division, under contract W-31-109-ENG-38.

References

- 1) Nuclear Structure, A. Bohr and B. Mottelson, (Benjamin, New York 1975) vII, p. 627
- 2) V. E. Viola, K. Kwiatkowski and M. Walker, Phys. Rev. C31, 1550 (1985)
- 3) A. J. Sierk, Phys. Rev. C33, 2039 (1986)
- 4) R. R. Betts, in Proceedings of Conference on Nuclear Physics with Heavy Ions, Stony Brook 1983, ed. P. Eraun-Munzinger (Harwood, New York 1984) p. 347
- 5) R. R. Betts, B. B. Back and B. G. Glagola, Phys. Rev. Lett. 47, 23 (1981)
- 6) S. Saini and R. R. Betts, Phys. Rev. C29, 1769 (1984)
- 7) R. R. Betts, S. B. DiCenzo and J. F. Petersen, Phys. Lett. 100B, 117 (1981)
- 8) R. W. Zurmühle, P. Kutt, R. R. Betts, S. Saini, F. Haas and Ole Hansen, Phys. Lett. 129B, 384 (1983)
- 9) A. H. Wuosmaa, R. W. Zurmühle, P. H. Kutt, S. F. Pate and S. Saini, Phys. Rev. C41, 2666 (1990)
- 10) S. Åberg (private communication)
- 11) W. Nazarewicz and J. Dobaczewski, Phys. Rev. Lett. 68, 154 (1992)
- 12) S. Marsh and W. D. M. Rae, Phys. Lett. 180B, 185 (1986)
- 13) G. Leander and S. E. Larsson, Nucl. Phys. A239, 93 (1975)
- 14) T. M. Cormier, C. M. Jachcinski, G. M. Berkowitz, P. Braun-Munzinger, P. M. Cormier, M. Gai, J. W. Harris, J. Barrette and H. E. Wegner, Phys. Rev. Lett. 40, 924 (1978)
- 15) D. A. Bromley, J. A. Kuehner and E. Almquist, Phys. Rev. Lett. 4, 365 (1960)
- 16) B. R. Fulton, S. J. Bennett, C. A. Ogilvie, J. S. Lilley, D. W. Banes, W. D. M. Rae, S. C. Allcock, R. R. Betts, and A. E. Smith, Phys. Lett. 181B, 233 (1986)
- 17) K. A. Erb, R. R. Betts, M. H. Hindi, S. K. Korotky, P. P. Tung, M. W. Sachs, S. T. Willett and D. A. Bromley, Phys. Rev. C 22, 507 (1980)
- 18) B. R. Fulton, S. J. Bennett, M. Freer, J. T. Murgatroyd, G. J. Gyapong, J. S. Jarvis, C. D. Jones, D. L. Watson, J. D. Brown, W. D. M. Rae, A. E. Smith and J. S. Lilley, Phys. Lett. B267, 325 (1991)

- 19) A. H. Wuosmaa, R. R. Betts, B. B. Back, M. Freer,
B. G. Glagola, T. Happ, D. J. Henderson, P. Wilt, and
I. G. Bearden, Phys. Rev. Lett. 68, 1295 (1992)

- 20) A. H. Wuosmaa, P. Wilt, R. R. Betts, B. B. Back, M. Freer,
B. G. Glagola, Th. Happ, D. J. Henderson, I. G. Bearden,
R. W. Zurmühle, D. P. Balamuth, S. Barrow, D. Benton, Q. Li,
Z. Liu and Y. Miao, Nucl. Inst. and Meth. (submitted)

END

**DATE
FILMED**

8 / 26 / 92

